Adaptive mesh in global magnetosphere simulation: Comparisons with global convection

Pekka Janhunen and Olaf Amm

Finnish Meteorological Institute, Geophysical Research, FIN-00101, Helsinki, Finland

Raymond A. Greenwald

Johns Hopkins University, Applied Physics Laboratory, Laurel, MD 20723, USA

Abstract. We present our newest adaptive multiscale MHD octogrid simulations of the coupled magnetosphere-ionosphere system using measured solar wind data as input. The resulting ionospheric convection patterns are compared with global SuperDARN measurements in various phases of a substorm and for various IMF orientations. The ionosphere is modelled as an electrostatic system obeying Ohm's law and current continuity. The ionospheric conductivity tensor depends on electron precipitation thus providing a feedback to the ionosphere-magnetoshere interaction. We review the still remaining weaknesses and poorly understood points of the model, the most important of which concern electron precipitation physics and the filling of the loss cone.

1. Introduction

In this paper we compare our GUMICS-3 global MHD simulation results with global SuperDARN [*Greenwald et al.*, 1995a] radar observations. The simulation code as used in this work is described in *Janhunen* [1996]. It uses first order Godunov-type finite volume method with explicit internal field separation, subcycling in time, an adapted hierarchical Cartesian mesh and projection scheme for $\nabla\cdot\mathbf{B}$ removal. Here we just write down briefly the equations which are solved in the simulation. The MHD equations used in the magnetosphere are

$$\frac{\partial\rho}{\partial t} = -\nabla\cdot(\rho\mathbf{v}), \tag{1}$$

$$\frac{\partial\mathbf{p}}{\partial t} = -\nabla\cdot\left(\frac{\mathbf{pp}}{\rho} + (P + \frac{B^2}{2\mu_0})\underline{\underline{\mathbf{1}}} - \frac{1}{\mu_0}\mathbf{BB}\right) \tag{2}$$

$$\frac{\partial u}{\partial t} = -\nabla\cdot\left[(u + P - \frac{B^2}{2\mu_0})\frac{\mathbf{p}}{\rho} + \frac{1}{\mu_0}(\mathbf{B}\times\frac{\mathbf{p}}{\rho}\times\mathbf{B})\right], \tag{3}$$

$$\frac{\partial\mathbf{B}}{\partial t} = -\nabla\times\mathbf{E} \tag{4}$$

$$\nabla\cdot\mathbf{B} = 0. \tag{5}$$

We have performed runs both with and without the Hall term in Ohm's law and the difference was not essential for the results presented in this paper. Ohm's law with the Hall term included is

$$\mathbf{E} + \mathbf{v}\times\mathbf{B} - \frac{1}{en}\mathbf{j}\times\mathbf{B} = 0. \tag{6}$$

The current density is defined by

$$\mathbf{j} \equiv \frac{1}{\mu_0}\nabla\times\mathbf{B} \tag{7}$$

and the relationship between the total energy density u and thermal pressure P is

$$P \equiv (\gamma - 1)\left(u - \frac{\mathbf{p}^2}{\rho} - \frac{\mathbf{B}^2}{2\mu_0}\right). \tag{8}$$

The quantity $\mathbf{p}$ is the momentum flux, $\mathbf{p} \equiv \rho\mathbf{v}$ and γ is the adiabatic constant ($\gamma = 5/3$ in this study).

In the ionosphere plane the continuity equation is

$$-\nabla\cdot\left(\Sigma_P\nabla\Phi_i + \Sigma_H\hat{\mathbf{b}}\times\nabla\Phi_i\right) = j_\parallel^{(i)}\sin I, \tag{9}$$

where the height-integrated Pedersen and Hall conductivities are obtained from a 3D electron density n by

$$\Sigma_{P,H} = \int dh F_{P,H} n \tag{10}$$

where $F_{P,H}$ are some precomputed coefficient tables. We have 20 height levels in our 3D ionospheric grid. The 3D electron density n is computed from

$$\frac{\partial n}{\partial t} = q - \alpha n^2, \tag{11}$$

where $q = Q(\rho, T, \Phi_m - \Phi_i)$ is the production term which depends on the source plasma density, temperature and ionosphere-magnetosphere potential difference. The functional form of Q is based on the MSIS-86 neutral atmospheric model [*Hedin*, 1987]. The details will not be given here.

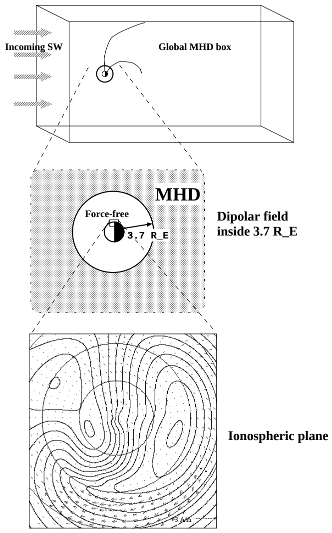

Figure 1. The overall structure of the GUMICS-3 simulation. The region inside $3.7R_E$ is not simulated by MHD equations but quantities are mapped along field lines.

The employed current-voltage relationship is given by

$$\Delta\Phi = \min\left(0, \frac{j_{\|}^{(i)}}{K} + \frac{k_B T}{e}\right) \tag{12}$$

where $j_{\|}^{(i)}$ is positive downward. Here K is the Lyons-Evans-Lundin constant, computed from

$$K = \frac{\chi n e^2}{\sqrt{2\pi m_e k_B T_e}}. \tag{13}$$

The dimensionless factor χ is the loss-cone filling rate. It is a dimensionless number between 0 and 1 which models the filling of the loss cone of magnetospheric electrons during one electron bounce period. When χ is zero, the loss cone is empty and there is no precipitation (and no field-aligned current), when it is unity the loss-cone filling is complete. Unfortunately we cannot compute the loss-cone filling rate self-consistently within MHD. However, we know that χ should be unity within the polar cap (i.e., in open field-line regions) because the plasma there hasn't been affected by ionospheric losses before. On the other hand, χ should be small in the radiation belts, otherwise there would be too large precipitation and bright auroras at too low latitudes (e.g., in Helsinki (!)). In this study we used the model

$$\chi = 0.01 + 0.99 \times \frac{1}{2}\left[1 + \tanh\left(\frac{\mathrm{INVLAT} - 67}{6}\right)\right] \tag{14}$$

[*Olsson*, 1997,] for the loss-cone filling rate.

The overall structure of the simulation is shown schematically in Figs. 1 and 2.

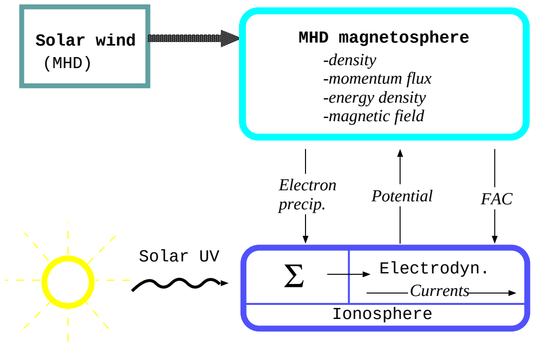

Figure 2. Schematic figure of the ionosphere-magnetosphere coupling implemented in GUMICS-3.

2. Simulation Setup

We use WIND plasma and IMF data for November 17, 1996, 16-22 UT.

In Fig. 3 we have plotted the IMF data as well as plasma data for this interval. The interesting period in this study is from 19:00 to 20:00.

In Figs. 4 and 5 we show the northern hemisphere ionospheric plane for slightly negative and positive IMF B_z, respectively. Fig. 4 shows a two-cell convection pattern, which is very typical (in the simulation, but also in observational data [*Lu et al.*, 1994; *Greenwald et al.*, 1995b; *Heppner and Maynard*, 1987]) for zero or slightly negative IMF B_z conditions. Fig. 5 shows a more complicated convection pattern with three or four cells, which is typical to northward IMF B_z orientation.

3. Comparison with SuperDARN Radar

Fig. 6 shows the simulated situation at 19:01 UT. A corresponding SuperDARN view is displayed in Fig. 7. The positions of the arrows in the SuperDARN plot indicate data points where at least one directional Doppler velocity estimate was obtained. The contour lines are a result of a spherical harmonic fitting to the data points and the arrow directions and lengths correspond to the fitted potential.

Generally, the simulation represents the measured SuperDARN potential patterns well for 19:01 and 19:29 UT. At 19:01, with negative IMF B_z and small IMF B_y, a two-cell pattern is visible with the cleft almost pointing to the noon direction. (Note that the two potential maxima on the morningside in Fig. 7 are most likely a

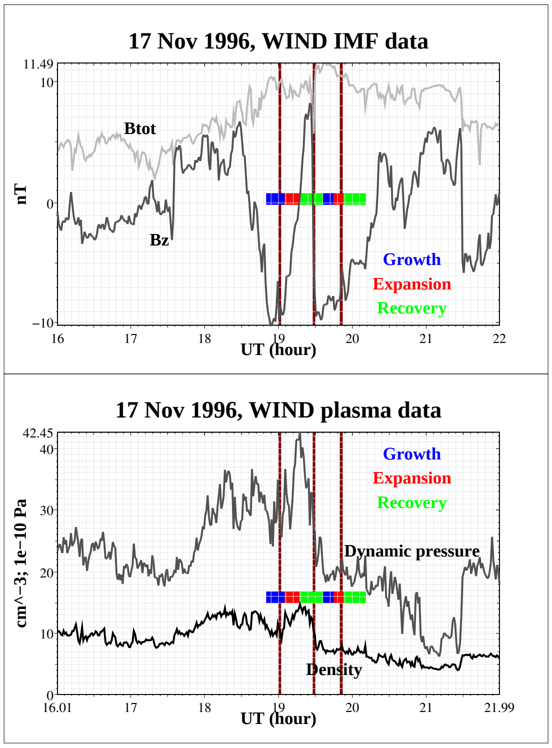

Figure 3. Input to the GUMICS-3 simulation is the solar wind data of Nov 17 1996 produced by the WIND spacecraft [data obtained from CDAWeb]. Times of display in Figs. 6–11 are marked with vertical lines (19:01, 19:29, 19:51). Substorm phases have been identified from simulation by looking at the motion of the neutral line.

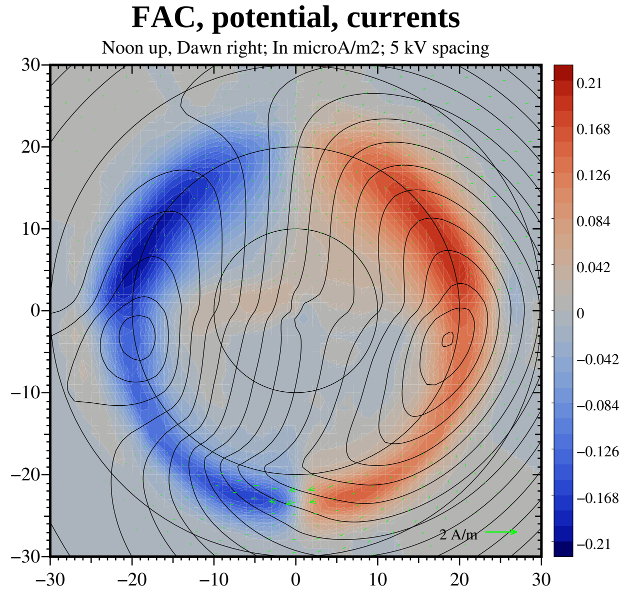

Figure 4. Simulation result for slightly negative IMF B_z, 17:10 UT. The potential contour lines show the ionospheric convection in the co-rotating frame of reference with 5 kV spacing. The small kink at the magnetic pole is of numerical origin. The shading shows the field-aligned current density. The field-aligned current (FAC) on the dawnside (right) is down (red in the original color figure). On the duskside (left) the FAC is upward (blue in the original figure).

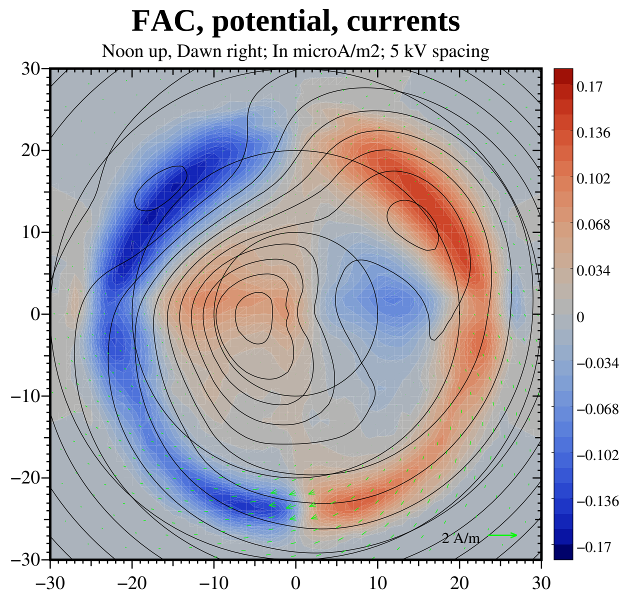

Figure 5. Same as Fig. 4 but for positive IMF B_z (18:05 UT).

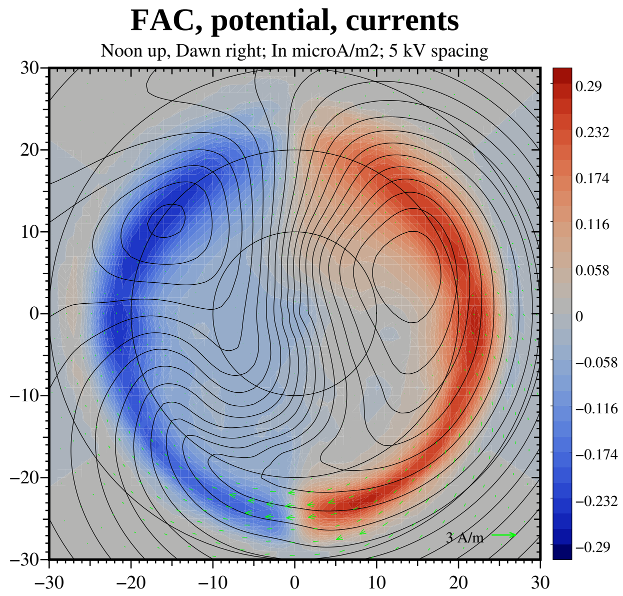

Figure 6. Same as Fig. 4 but for strongly negative IMF B_z (19:01 UT).

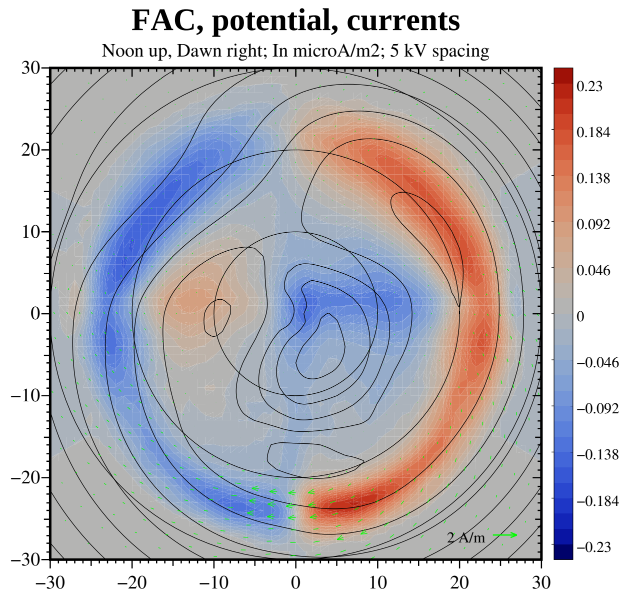

Figure 8. Same as Fig. 4 but after a positive excursion in IMF B_z (19:29 UT).

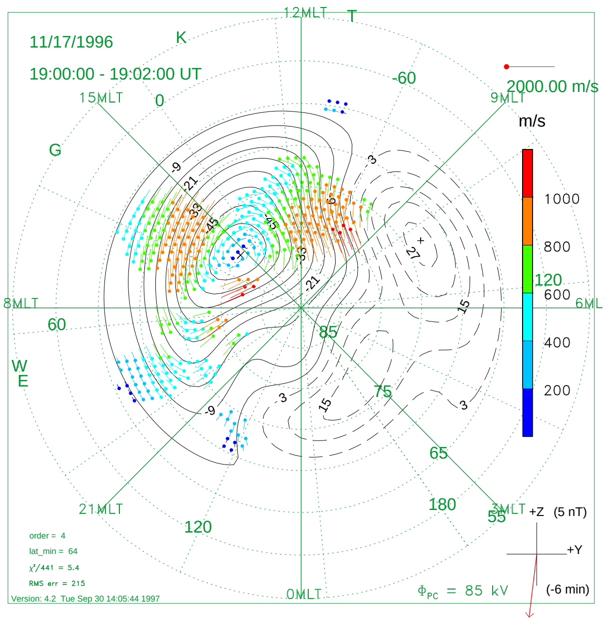

Figure 7. The SuperDARN view corresponding to Fig. 6.

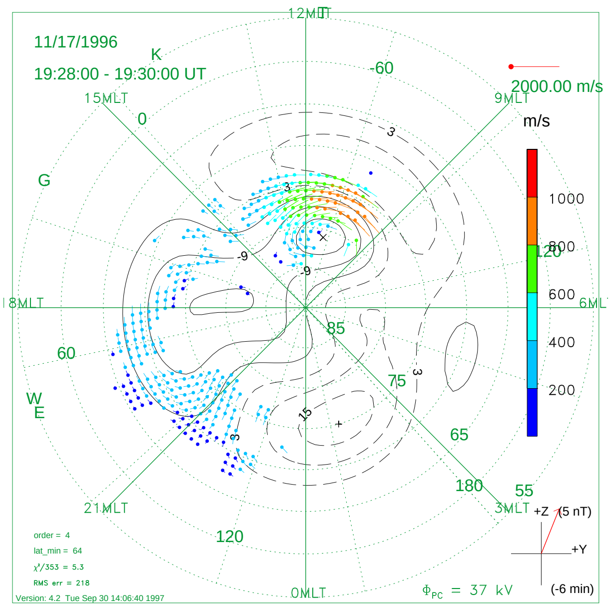

Figure 9. The SuperDARN view corresponding to Fig. 8.

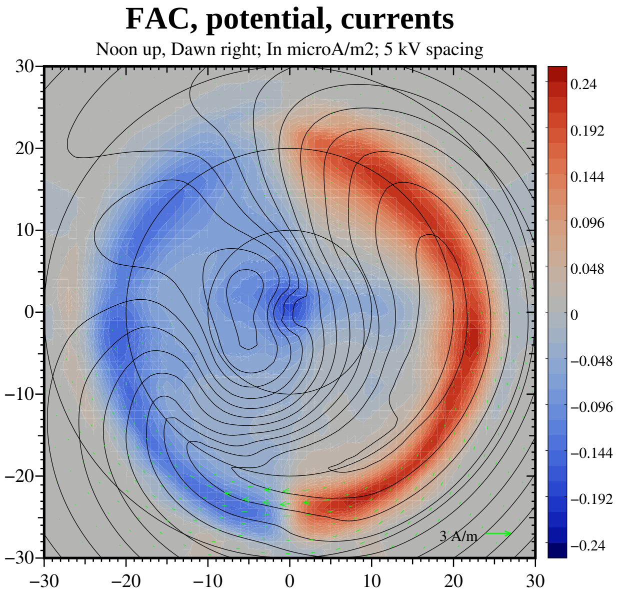

Figure 10. Same as Fig. 4 but for 19:51 UT.

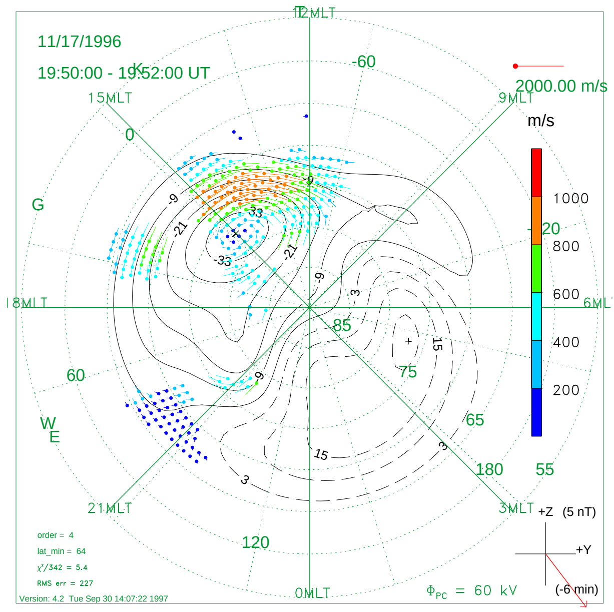

Figure 11. The SuperDARN view corresponding to Fig. 10.

consequence of the spherical harmonic fit, since nearly no radar data is available in the morning sector in this case.) The potential difference between morning and evening side extrema (the polar cap potential drop) is 85 kV in SuperDARN and 100 kV in the simulation, thus the agreement is also quantitatively good.

Figs. 8 and 9 show a similar comparison for 19:29 UT. This is a positive IMF B_z period, and a multicell potential structure is seen in both SuperDARN and in the simulation. Around a potential maximum near the magnetic pole, there are two minima in the early noon and midnight sector, and another small maximum at 18 MLT and 80 deg. magnetic latitude. The max-min potential difference is 37 kV in SuperDARN and 30 kV in the simulation, thus the agreement is good also in this case.

Finally, in Figs. 10 and 11 we show a comparison near the end of the simulation, 19:51 UT. At this stage the agreement is not very good, and the probable reason is that after all those abrupt changes in the solar wind parameters and the substorm activity, the simulation has "lost its track" and drifted farther from reality than in the earlier stages. The situation is messy, and probably quite sensitive to small changes in the input data. However, it is interesting that the agreement in the max-to-min potential difference (60 and 65 kV in SuperDARN and simulation, respectively) is very good in this case as well, even if the details are wrong.

4. Deficiencies of the Simulation

The simulation model presented here is already quite comprehensive. It can produce the dynamical behavior of the whole magnetosphere-ionosphere system based on just the measured time series of solar wind plasma parameters and magnetic field. However some problem areas still remain. The most important shortcomings of the simulation model presented in this paper are the following.

- The ionosphere-magnetosphere coupling in general (i.e., the physics behind Eqs. (12) and (13)), are still physically poorly understood [*Janhunen*, 1998, e.g.,]. For example, it is unclear what value of K one should use in return current regions. Some recent results [*Janhunen and Olsson*, 1998] indicate that the whole concept of auroral acceleration may need to be revised.

- Ionospheric plasma outflow is currently not included in the simulation. This is related to the previous point.

- The loss cone filling rate is not self-consistently computed. This is also tightly related to the previous two points.

- The dipole must not be tilted. This restriction will be removed in near future (see below).

- We are currently not taking into account IMF B_x in order to avoid generating a $\nabla \cdot \mathbf{B} \neq 0$ condition on the inflow boundary. We are presently considering various ways to remove this deficiency also. Some of the other groups doing global MHD simulations have seemingly resolved this problem already.

- The tail length produced by the MHD simulation seems to be shorter than in reality. This is true for our simulation as well as for some other global ideal MHD simulations that we are aware of (Tamas Gombosi, private communication). One could think that turbulent viscosity (eddy viscosity) should be modelled and added to the global MHD equations. This might make the tail longer without producing unwanted resistivity.

As seen, most of the problem areas are no longer related to MHD or numerical accuracy, but to the physics of ionosphere-magnetosphere coupling.

5. Summary and Future Research

Let us summarize our main results.

- On the dayside the agreement between simulation and radar is often quite good. This holds for both positive and negative IMF B_z. This is not surprising, since the dayside is more directly affected by the solar wind and thus it is natural that an MHD simulation can reproduce such cases well (tail dynamics plays no role). Also the SuperDARN radar works best on the dayside because the ionospheric electron density is more uniform and does not cause unpredictable ray paths as may happen on the nightside.

- On the nightside the agreement is not always very good. Inadequancies in the simulation manifest themselves more easily on the nightside, because the tail dynamics is heavily involved. Also the SuperDARN radar has fewer usable data points there, which makes the comparison more difficult. For example, the location of the Harang discontinuity in Fig. 6 is somewhat different from results obtained by measurements [*Amm*, 1998].

- After many turnings of the IMF, the simulation and observation lose coherence, at least temporarily. This shows the limits of the current simulation accuracy and indicates that the later substorms in substorm sequences are increasingly sensitive to boundary conditions, which is not surprising.

- There is good quantitative agreement in the magnitude of the potential between simulation and SuperDARN all the time, even in cases where there is some disagreement in convection cell locations.

Future Research. We are now preparing a new code whose main new feature is cell-by-cell automatic grid adaptation. When this code runs in production, we will be able to fully take into account tilted dipole conditions, which is important for effective event studies.

This paper can be accessed as an online version (with color figures) at the following URL: `http://www.geo.fmi.fi/~pjanhune/papers/Portugal98/`.

References

Amm, O., Method of characteristics in spherical geometry applied to a Harang discontinuity situation, *Ann. Geophysicae,* 16, 413, 1998.

Greenwald, R. A., Baker, K. B., Dudeney, J. R., Pinnock, M., Jones, T. B., Thomas, E. C., Villain, J.-P., Cerisier, J.-C., Senior, C., Hanuise, C., Hunsucker, R. D., Sofko, G., Koehler, J., Nielsen, E., Pellinen, R., Walker, A. D. M., Sato, N., Yamagishi, H. DARN/SuperDARN: A global view of the dynamics of high-latitude convection, *Space Sci. Rev.,* 71, 761-796, 1995.

Greenwald, R. A., Bristow, W. A., Sofko, G. J., Senior, C., Ceriser, J.-C., Szabo, A., Super Dual Auroral Radar Network radar imaging of dayside high-latitude convection under northward interplanetary magnetic field: Toward resolving the distorted two-cell versus multicell controversy, *J. Geophys. Res.*, 100, 19661-19674, 1995.

Hedin, A.E., MSIS-86 atmospheric model, *J. Geophys. Res.,* 92, 4649, 1987.

Heppner, J.P. and N.C. Maynard, Empirical high-latitude electric field models, *J. Geophys. Res.*, 92, 4467, 1987.

Janhunen, P., GUMICS-3 – a global ionosphere-magnetosphere coupling simulation with high ionospheric resolution, Proc. Environmental Modelling for Space-Based Applications, 18-20 Sept. 1996, ESTEC, The Netherlands, ESA SP-392, 1996.

Janhunen, P. and Koskinen, H.E.J., The closure of Region-1 field-aligned current in MHD simulation, *Geophys. Res. Lett.* **24**, 1419–1422, 1997.

Janhunen, P., On the current-voltage relationship in fluid theory, *Ann. Geophysicae,* in press, 1998.

Janhunen, P. and Olsson, A., Comparisons of current-voltage and energy flux relationships based on O- and U-shaped potential models, *Ann. Geophysicae,* submitted, 1998.

Lu, G., A.D. Richmond, B.A. Emery, P.H. Reiff, O. de la Beaujardiere, F.J. Rich, W.F. Denig, H.W. Kroehl, L.R. Lyons, J.M. Ruohoniemi, E. Friis-Christensen, H. Opgenoorth, M.A.L. Persson, R.P. Lepping, A.S. Rodger, T. Hughes, A. McEwin, S. Dennis, R. Morris, G. Burns and L. Tomlinson, Interhemispherical asymmetry of the high-latitude ionospheric convection pattern, *J. Geophys. Res.,* 99, 6491–6510, 1994.

Olsson, A., Studies of magnetosphere-ionosphere couling in auroral substorms using radar and satellite techniques, *Ph D* thesis, IRF Scientific Report 240, Kiruna, 1997.